Hindawi
Shock and Vibration
Volume 2023, Article ID 9813172, 1 page
https://doi.org/10.1155/2023/9813172

Retraction

Retracted: Mining Stress Distribution in Stope and Overlying Rock Fracture Characteristics and Its Disaster-Pregnant Mechanism of Coal Mine Earthquake

Shock and Vibration

Received 17 October 2023; Accepted 17 October 2023; Published 18 October 2023

This article has been retracted by Hindawi following an investigation undertaken by the publisher [1]. This investigation has uncovered evidence of one or more of the following indicators of systematic manipulation of the publication process:

(1) Discrepancies in scope

(2) Discrepancies in the description of the research reported

(3) Discrepancies between the availability of data and the research described

(4) Inappropriate citations

(5) Incoherent, meaningless and/or irrelevant content included in the article

(6) Peer-review manipulation

The presence of these indicators undermines our confidence in the integrity of the article's content and we cannot, therefore, vouch for its reliability. Please note that this notice is intended solely to alert readers that the content of this article is unreliable. We have not investigated whether authors were aware of or involved in the systematic manipulation of the publication process.

Wiley and Hindawi regrets that the usual quality checks did not identify these issues before publication and have since put additional measures in place to safeguard research integrity.

We wish to credit our own Research Integrity and Research Publishing teams and anonymous and named external researchers and research integrity experts for contributing to this investigation.

The corresponding author, as the representative of all authors, has been given the opportunity to register their agreement or disagreement to this retraction. We have kept a record of any response received.

References

[1] P. Lyu, K. Lu, and X. Chen, "Mining Stress Distribution in Stope and Overlying Rock Fracture Characteristics and Its Disaster-Pregnant Mechanism of Coal Mine Earthquake," *Shock and Vibration*, vol. 2022, Article ID 7606360, 17 pages, 2022.

Hindawi
Shock and Vibration
Volume 2022, Article ID 7606360, 17 pages
https://doi.org/10.1155/2022/7606360

Research Article

Mining Stress Distribution in Stope and Overlying Rock Fracture Characteristics and Its Disaster-Pregnant Mechanism of Coal Mine Earthquake

Pengfei Lyu,[1] **Kangbin Lu**,[1] **and Xuehua Chen**[2]

[1]*School of Mining and Coal Engineering, Inner Mongolia University of Science and Technology, Inner Mongolia, Baotou 014000, China*
[2]*College of Mining, Liaoning Technical University, Fuxin 123000, Liaoning, China*

Correspondence should be addressed to Pengfei Lyu; 2018930@imust.edu.cn

Received 8 September 2022; Accepted 10 October 2022; Published 21 November 2022

Academic Editor: Leibo Song

The corresponding engineering effects are inevitable and occurred when the coal mines working face mining. The main manifestations are distribution of mining stress and fracture of overlying rock seams. The mining effects play a controlling role in the occurrence of dynamic disasters such as disastrous coal mine earthquakes and rock bursts. In view of this, taking No. 1305 working face mining of Dongtan coal mine for background, the distribution and transfer characteristics of mining stress in working face and fracture characteristics of roof rock formation were studied by theoretical analysis, numerical simulation, and microseismic monitoring. The change mechanism of stress, strain, strain rate, and energy of rock mass in the process of coal mine earthquake gestation was expounded by the Burgers mechanical model. The results show that the microseismic hypocenters are mainly concentrated near the increasing pressure zone and the fractured zone. The hypocenter first gathered at the main roof, and then, it gradually developed upward and returns to the main roof after mining. The distribution of microseismic frequency and advanced support pressure is basically consistent. The microseismic energy peak value area with respect to the support pressure peak value area often presented a certain lag. The relationship of empirical formula is inferred as $Y_E = M_E + \Delta d$. The overlaying rock caving zone and fractured zone with height of 37.8 m and 95 m, respectively, were revealed by microseismic monitoring. It is 8.4% larger than the numerical result. It shows that the prediction results of overlying rock fracture height based on the distribution of large energy hypocenter points is well applied in the field, and the operations are simple and intuitive.

1. Introduction

China is one of the most serious coal mine dynamic destinations in the world [1]. At present, there are 241 rock burst mines in 26 coal-producing provinces, cities, and autonomous regions in China. It is mainly distributed in Shandong, Henan, Heilongjiang, Jilin, Inner Mongolia, and other provinces, cities, and autonomous regions [2, 3]. There are more than 1000 severe dynamic-appearing mines accompanied by the induced strong coal mine earthquakes during coal mining [4, 5]. In recent years, with the extension of coal mining to the deep, the number of rock burst mines continued to increase and the degree of rock burst danger continued to strengthen. Although the China coal enterprises carry out the regional and local measures to prevent and control rock burst. The large coal mine earthquakes and rock burst accidents still occurred every year. For example, the "10.20" rock burst accident was occurred in Heze city, Shandong province in 2018. The "6.9" rock burst accident occurred in Liaoyuan city, Jilin province, in 2019 and the "2.22" rock burst accident occurred in Heze city, Shandong province, in 2020 [6–8]. On the one hand, the frequent occurrence of mine dynamic disasters such as the coal mine earthquake and rock burst was related to geological construction movement of coal-bearing stratum; on the other hand, it was related to the attribute of the coal seam and

mining method [9, 10]. Therefore, the mining engineering effects such as the mining-stress distribution and transfer, overburden fractures in the working face mining were analyzed in detail. It is the foundation and key to study mechanism of prevention and control of a dynamic disaster.

The corresponding engineering effects were inevitable and occurred when the mines working face mining. The typical mining engineering effects include secondary distribution characteristics of mining stress and overburden movement characteristics [11–13]. The complex and changeable engineering effect was caused by mining in stope. The mechanical balance system consisting of the coal seam, roof, and floor are always changing when the working face is advancing [14, 15]. Such as the advance support pressure, lateral pressure, and height of overlying rock of three zones were changed when the working face mining. The disasters of coal mine earthquake and rock burst were induced when the mining engineering effects reach or exceed critical state destruction of the coal-rock medium. Although the research studies for mining engineering effect of working face started earlier, due to the special working conditions of mine production, many conventional methods were not achieving desired results in the mine production and scientific research. Therefore, the research of mining engineering effect in mine working face and its control role of formation mechanism of dynamic disasters still have a long way to go.

The representative research results of mining engineering effects mainly included the following points of view. Wang et al. [16–18]; according to the movement characteristics of the "surrounding rock - coal body" system, the mining instability model of overlying rock structure "one big and two small" was established, and the conclusion was verified by microseismic monitoring. Pan et al. [19, 20] described the whole evolution process of lateral support pressure in goaf based on microseismic monitoring data. It is considered that the microseismic distribution along the coal rib presented the reverse "C" shape. The intensity of microseismic activity on both the sides is preferable than the middle of the working face. Kong et al. [21] analyzed the surrounding rock failure of overlying strata, movement, and support pressure distribution of law by microseismic monitoring. It is considered that mining stress transfer was caused by the fundamental of surrounding rock failure. Wang et al. [22–25]; according to the results of coal body stress monitoring, the vertical stress distribution law of double roadway layout working face were interpreted, and it is considered that the vertical stress of coal seam presents five stage characteristics in strike. Based on this, the elastic-plastic evolution law of coal seam was studied. Cai et al. [26–28] the P wave velocity in 25110 working face of the Yuejin coal mine in Henan province was carried out the inversion by combining tomography technique with real-time microseismic monitoring, and the assessment of rock burst risk was performed successfully. Gao et al. [29] using the microseismic monitoring technology, the whole process of coal-rock gas compound dynamic disaster was monitored. At present, the microseismic monitoring technology is an important means to study the coal, rock, and gas compound dynamic disaster. It is the great significance to study the mechanism of coal, rock, and gas compound dynamic disaster and its previous identification. The typical studies on the effect of mining engineering and mechanism of coal mine earthquake and rock burst also include references [30–36]. These studies mainly used the numerical simulation, theoretical analysis, field tests, and laboratory experiments. The adverse engineering effects were caused by working face mining, and the mining control mechanism of coal mine earthquake and rock burst were revealed from the perspectives of mining overlying rock structure, advanced support pressure, lateral pressure, and elastic-plastic deformation.

The abovementioned results lay a good foundation for further research. In this paper, the author systematically analyzes the relationship between microseismic hypocenter, frequency, energy, and mining engineering effects by microseismic monitoring data, and allows the numerical simulation to verify it. Finally, the mechanical mechanism of coal mine earthquake gestation was revealed from the perspective of change law of mining stress, strain, energy, and strain rate.

2. Layout of the Microseismic Monitoring System

2.1. Geological Survey and Mining Technology of the Dongtan Coal Mine. The Dongtan coal mine is a large modern comprehensive mechanized mining mine in China and it is located in the east of the Yanzhou coalfield. The geotectonic location of the Yanzhou coalfield lies in southwest margin of the West China platform anticline and the east of Jining graben in the southwest Shandong fault block depression. The Yanzhou coalfield can be divided into the miocene group, basement structural layer, and palaeozoic group with two caprock structural layers from a longitudinal structural layer. The construction movement was mainly affected by Taishan movement, and the construction change of the caprock structural layer is mainly affected by Yanshan movement. The Dongtan coal mine is located in the middle part of Yanzhou syncline. It is mainly the broad-gentle folds and a certain number of moderately developed faults. The western structure of minefield is relatively simple. The eastern fault is more developed. The fault is very developed in the area near the Yishan fault and influence of the Yishan fault. The serious dynamic phenomena and construction stress concentrated of Dongtan coal mine may induce during the coal seam mining.

Dongtan coal mine is one of the most serious coal mine earthquake and rock burst disasters in China. The main mining No. 3 coal seam in minefield has the weak shock tendency. The local regional of No. 3 coal seam bifurcation is 3_{upper} and 3_{lower} coal seam. The coal seam thickness is 5.3–12.2 m. The average thickness is 8.6 m. The dip angle is 0–6°. The immediate roof of the coal seam is dominated by siltstone mixed with the certain mudstone, fine sandstone, and medium sandstone. The roof is smooth and has good integrity. The fractures were not developed. The main roof is the thick medium sandstone, the thick fine sandstone, the calcium, and the siliceous cementation with height of 10–20 m. The compressive strength is 90–130 MPa. The floor

is generally the dark gray siltstone. The coal mining method is a high power fully mechanized mining and fully mechanized top coal caving method, and the all falling method is used to manage the roof.

2.2. Microseismic Monitoring System and Sensor Layout. In order to predict the dynamic response of coal-rock mass during mining, a set of the Poland SOS was introduced in Dongtan coal mine since April 2010. The system hardware mainly includes two parts: the surface equipment and underground equipment. The surface part includes the UPS power supply, analyzer, recorder, and data acquisition station. The underground part includes the broadband coal mine earthquake wave shape special vibration pickup sensor and signal transmission cable. The analyzer is equipped with the SeisGram and Multilock signal processing software. It is used for the automatic calculation of microseismic parameters. The response frequency range of microseismic signal picked up by a seismic sensor of SOS among similar products is the widest and it is 0.1–600 Hz. The high and low energy microseismic signals were monitored at the same time. According to the layout principle of microseismic monitoring network [37], a total of 16 microseismic monitoring stations were arranged in the Dongtan coal mine, which mainly monitor the first mining section, fourth mining section, and fourteen mining section where the working face is excavated or mined. The microseismic events of effective monitoring were 4 or more stations from the actual monitoring situation, and mostly used P wave positioning. To ensure positioning accuracy, the minimum 4 stations receive microseismic signals regarded as an effective shock event. The positioning error of one-way system is less than 15 m, which satisfies the expected positioning accuracy. The location distribution of underground microseismic monitoring stations in the Dongtan coal mine is shown in Figure 1.

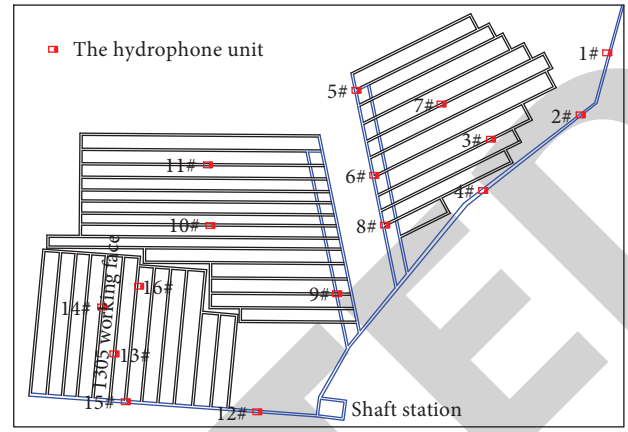

Figure 1: Microseismic monitoring station layout.

Lithology	Columnar	Thickness (m)
Siltstone		1. 80
Mudstone		0. 55
Fine-grained sandstone		1. 45
Sandy mudstone		1. 83
Medium-grained sandstone		14. 98
Sandy mudstone		5. 44
Siltstone		2. 45
Sandy mudstone		1. 12
The 3 coal		7. 60 (0. 15)
Sandy mudstone		3. 72
Mudstone		2. 69
Clay rock		1. 10
Siltstone		0. 50
Sandy mudstone		3. 51

Figure 2: Comprehensive columnar section of the coal seam.

3. Characteristics of the Mining Stress Distribution and Transfer

3.1. Survey of the Test Working Face and the Numerical Calculation Model. Taking the 1305 working face as the background, the stress distribution and transfer characteristics of working face mining were analyzed based on the method of combining microseismic monitoring and numerical simulation. The coal seam tectonic of the 1305 working face is simple. The thickness of coal seam is 7.1–8.1 m, the average is 7.6 m. The dip angle is 1–6°, and the average is 3°. The inclined length of the 1305 working face is 205 m. The advancing length is 752 m. The mining depth is 683–708 m and the average is 690 m. The roof of coal seam is mainly sandstone and mudstone. The Protodyakonov coefficient of rock formation is 4.7–15. The average thickness of the main roof (medium-grained sandstone) is 14.98 m and the thickness of local area can reach more than 25 m as shown in Figure 2.

Referring to the stratum distribution of the 1305 working face in Dongtan coal mine, the three-dimensional finite difference numerical model was established by the FLAC^{3D} software in stope in Figure 3. The top of model applied uniform load is 15.75 MPa. According to the results of in-situ stress test, the applied horizontal stress SXX is 25.1 MPa and SYY is 7.6 MPa. The round and the bottom adopt the fixed constraints, the Mohr–Coulomb yield criterion; the rock formation parameters in the model are shown in Table 1.

3.2. Relationship between Vertical Stress and Microseismic Sources. The mining of working face broke the original mechanical balance of underground rock mass. Most microseismic sources are located in the roof of coal seam and the fracture of coal seam roof is mainly caused by vertical stress. So, it is necessary to analyze the relationship between

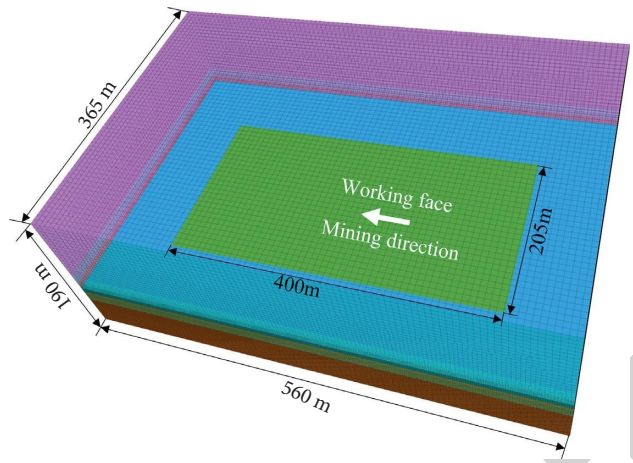

Figure 3: Three-bit grid division of the model.

Table 1: Physical and mechanical parameters of coal and rock.

Lithology	Density/ (kg•m^{-3})	Elasticity modulus/ GPa	Poisson ratio	Uniaxial compressive strength/MPa	Cohesion/ MPa	Internal friction angle/°
Siltstone	2630	11.47	0.26	7.74	13.72	41.17
Mudstone	1650	8.41	0.21	3.26	6.51	33.18
Medium-grained sandstone	2580	12.97	0.25	11.32	16.81	42.25
Sandy mudstone	1960	9.71	0.23	4.38	8.71	38.86
Coal	1430	2.21	0.21	1.12	1.96	30.48
Clay rock	1550	3.46	0.22	2.86	4.79	33.31

vertical stress and microseismic source distribution. For accurately analyzing the distribution and transfer characteristics of mining stress and its relationship with the microseismic hypocenter, the microseismic events were projected onto vertical stress distribution cloud map according to the actual geographical coordinates in Figure 4. It can be seen that the distribution of hypocenter points is completely regular. First, the hypocenter points were accumulated in front of working face and the goaf was gathered behind. The front of working face is more than goaf behind, and it mainly concentrated near the fracture zone and the vertical stress elevating zone. Second, the hypocenter point first accumulates at the main roof with working face advances. It gradually develops to the upper rock stratum during mining. The hypocenter of goaf again decreased to near the main roof after mining. The maximum value of vertical stress in front of coal rib is 10–16 m. The hypocenter points were mainly distributed in the vertical stress increasing and decreasing areas. However, the distribution is less in the stress stable region.

3.3. Relationship between Advance Support Pressure and Microseismic Energy. The numerical simulation results of the 1305 working face shows. The distance from the peak value of advance support pressure to the coal rib is about 10–16 m. The stress concentration coefficient is 1.2–2.4. This is basically consistent with the theoretical value. It also shows the numerical results are more accurate. To further analyze the relationship between range and peak value position of advanced support pressure and microseismic frequency and energy, the microseismic data were processed as follows. The distance of an effective sliding window is 4 m. Then, it displayed in the same picture with support pressure curve. The relationship between support pressure peak value area and microseismic energy and frequency extreme value area is shown in Figure 5.

The relationships between microseismic frequency, energy, and support pressure of working face from setup entry advanced to 400 m in Figure 5. It can be seen that the distribution trend of microseismic frequency and support pressure was basically consistent. The stress in the peak value area of advanced support pressure increases, coal-rock mass was seriously broken, the microseismic events increase, and the large coal mine earthquakes were gestated. At the same time, it also shows that the stress value has a good positive correlation with microseismic frequency. However, the nonstress peak value region was also the region where the high energy microseismic events occurred. The relationship diagram between microseismic energy and support pressure shows that the peak value energy region has a certain lag with respect to the peak value stress region. That is, the peak value energy often occurs at a certain distance behind the peak value stress. Therefore, the empirical formula of relationship between stress peak value position and energy peak value position can be preliminarily deduced to $Y_E = M_E + \Delta d$. The formula Y is the distance between peak value stress and coal rib, m. M_E is the distance between energy peak value and coal rib (positive on the solid coal side and negative on the goaf side), m. The Δd value is the distance of the both, m. According to the different factors such as the

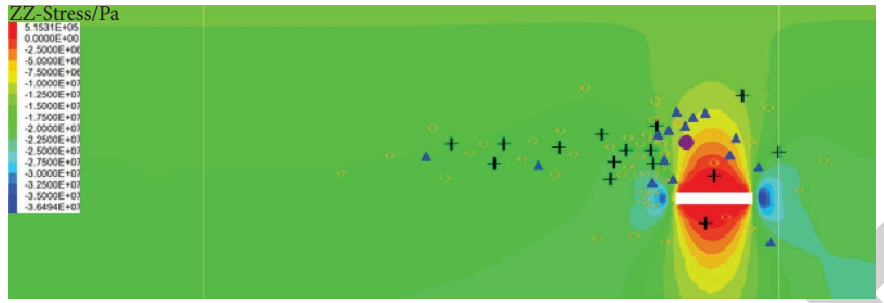

◇ 0.1-0.5 kJ ● 5-10 kJ

┼ 0.5-1 kJ ★ 10-50 kJ

▲ 1-5 kJ

(a)

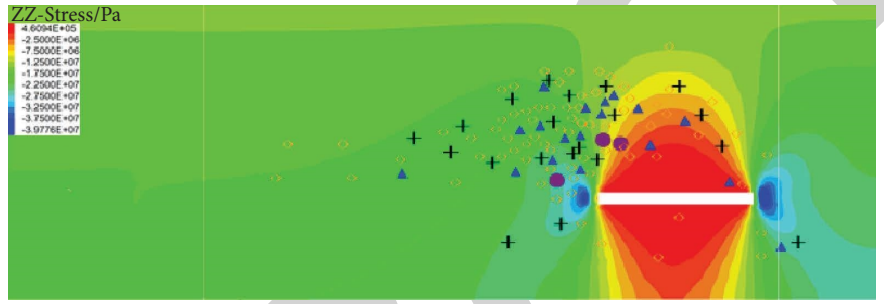

◇ 0.1-0.5 kJ ● 5-10 kJ

┼ 0.5-1 kJ ★ 10-50 kJ

▲ 1-5 kJ

(b)

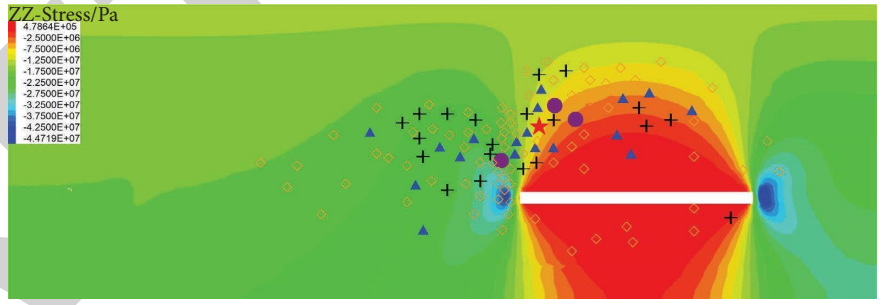

◇ 0.1-0.5 kJ ● 5-10 kJ

┼ 0.5-1 kJ ★ 10-50 kJ

▲ 1-5 kJ

(c)

Figure 4: Continued.

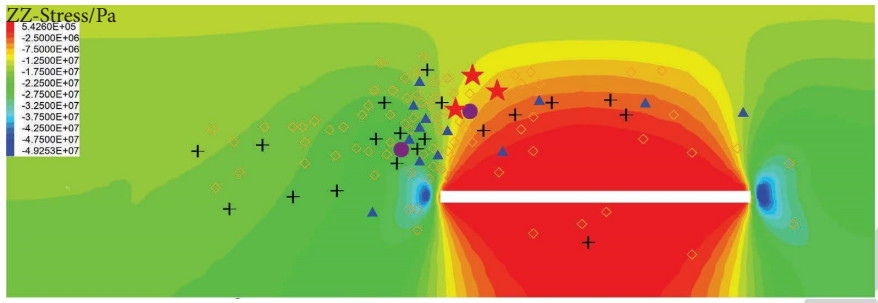

0.1-0.5 kJ 5-10 kJ
0.5-1 kJ 10-50 kJ
1-5 kJ

(d)

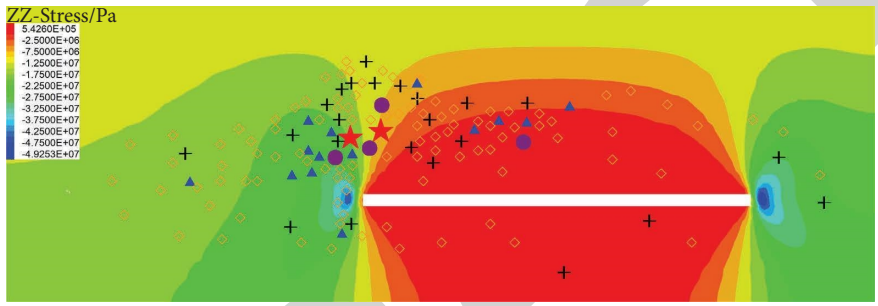

0.1-0.5 kJ 5-10 kJ
0.5-1 kJ 10-50 kJ
1-5 kJ

(e)

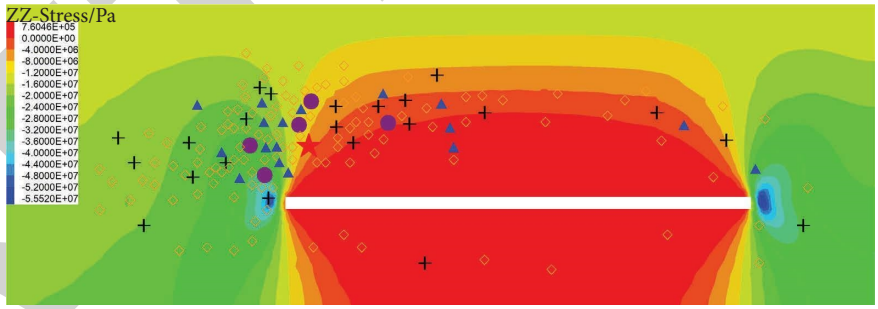

0.1-0.5 kJ 5-10 kJ
0.5-1 kJ 10-50 kJ
1-5 kJ

(f)

Figure 4: Continued.

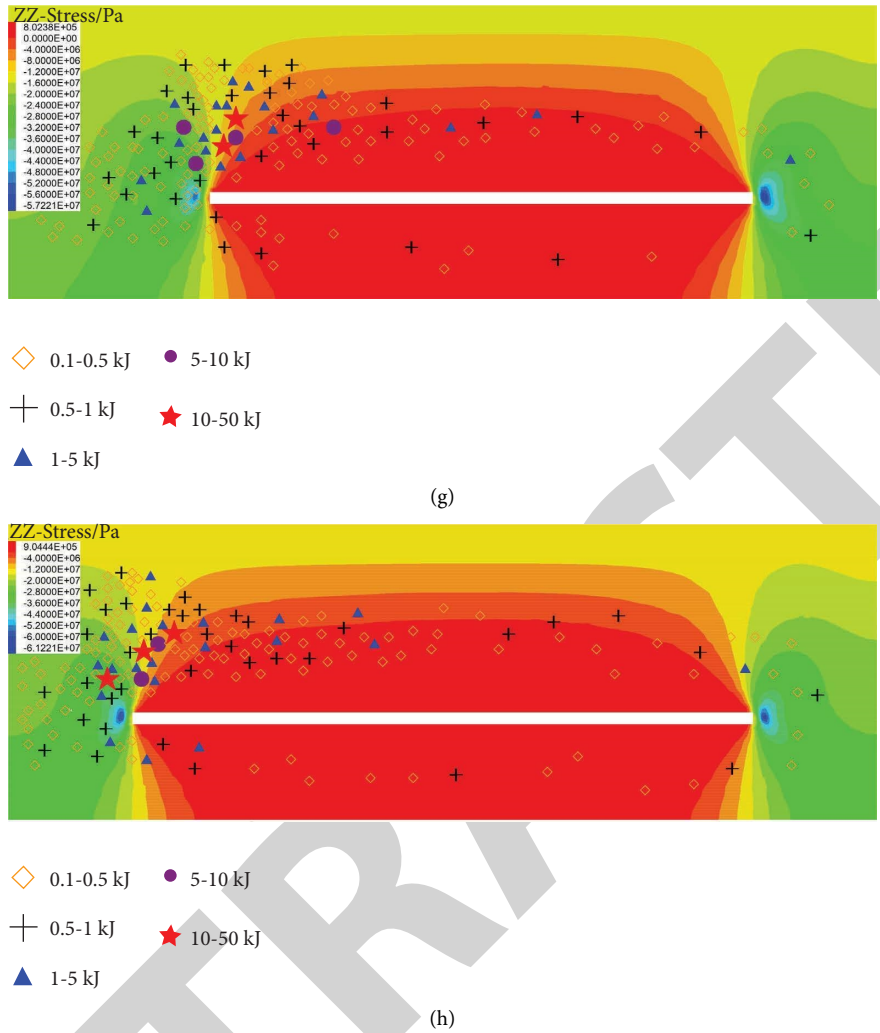

Figure 4: Distribution of microseismic events on vertical stress cloud. (a) Caving 50 m. (b) Caving 100 m. (c) Caving 150 m. (d) Caving 200 m. (e) Caving 250 m. (f) Caving 300 m. (g) Caving 350 m. (h) Caving 400 m.

coal seam thickness, roof lithology, period-to-press step distance, and mining methods, and others, the Δd value differences are also large. According to experience, it is generally 10–30 m. The Δd value of the 1305 working face in the Dongtan coal mine is 20 m after the calculation, statistics, and field investigation. In the mining process of other working faces, the location of high-energy coal mine earthquake can be inferred according to the law. The disastrous coal mine earthquake can be predicted.

4. Fracture Characteristics of Mining Overlying Rock Revealed by Microseismic Events

4.1. Stratified Statistical Results of Microseismic Events. The stratified statistics of microseismic events on the roof and floor of working face can reflect the concentrated location of coal mine earthquake disaster and energy release [38]. The aim was to provide a reference for explicating the trend of energy release and direction of pressure relief in advanced. Therefore, the floor, coal seam, immediate roof, and main roof of the 1305 working face in the Dongtan coal mine and the uppermost rock formation of microseismic number and energy percentage are counted in Figure 6. The part less than 0 in Figure 6 indicates the coal seam floor. It can be seen that the microseismic energy and frequency were mainly concentrated in the position of 40–70 m above the coal seam floor. This position is basically above the main roof. The lithology of rock formation in this horizon is a dark gray sandstone and it is mainly the hard fine sandstone. This indicates that the fracture of hard fine sandstone dominated the microseismic events of whole working face and released a lot of energy. Therefore, it is considered that this rock formation is the key stratum to control the occurrence of coal mine earthquakes in the 1305 working face.

4.2. Two-Zone Height of Overlying Rock Revealed by Microseismic Events. The mining stress field changes at any time and the stress concentration area has the real-time movement when working face mining. The mining stress field and in-situ stress field superposition and increases sharply; in some areas, it formed in different levels of shock

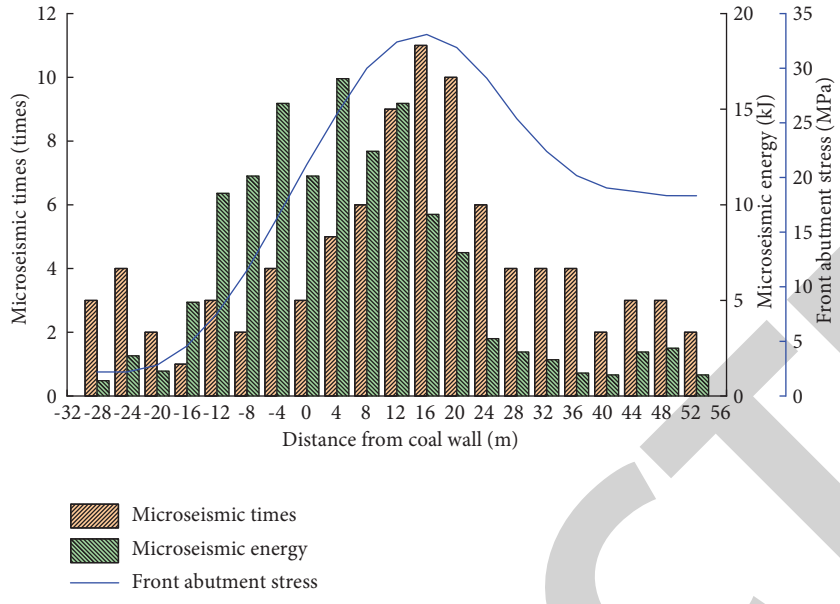

(a)

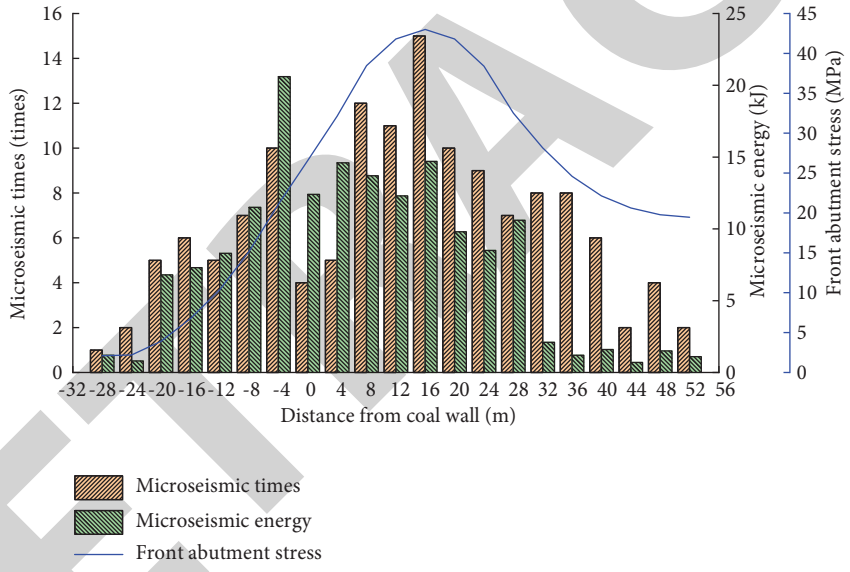

(b)

Figure 5: Continued.

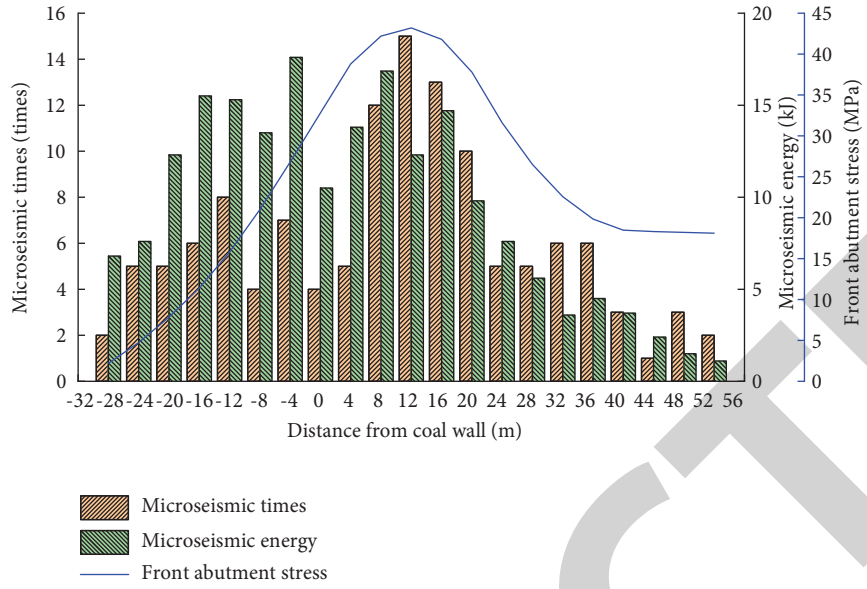

(c)

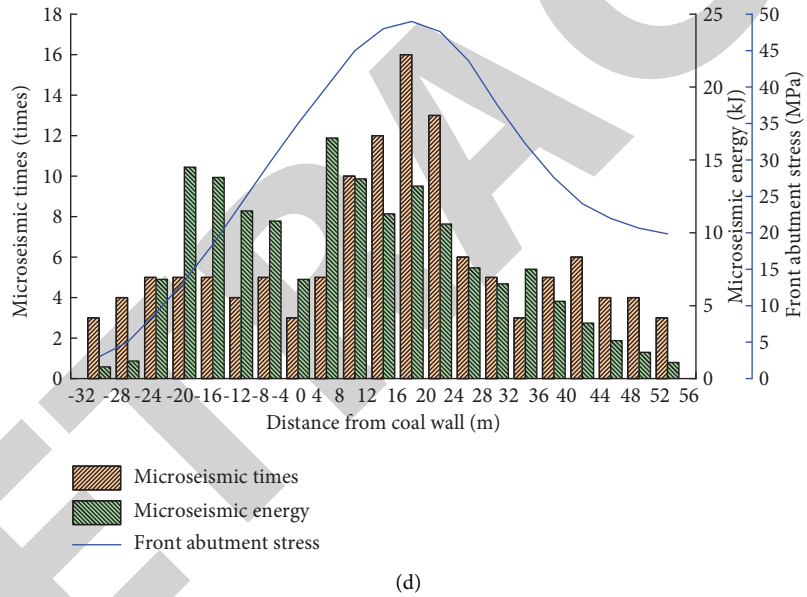

(d)

Figure 5: Continued.

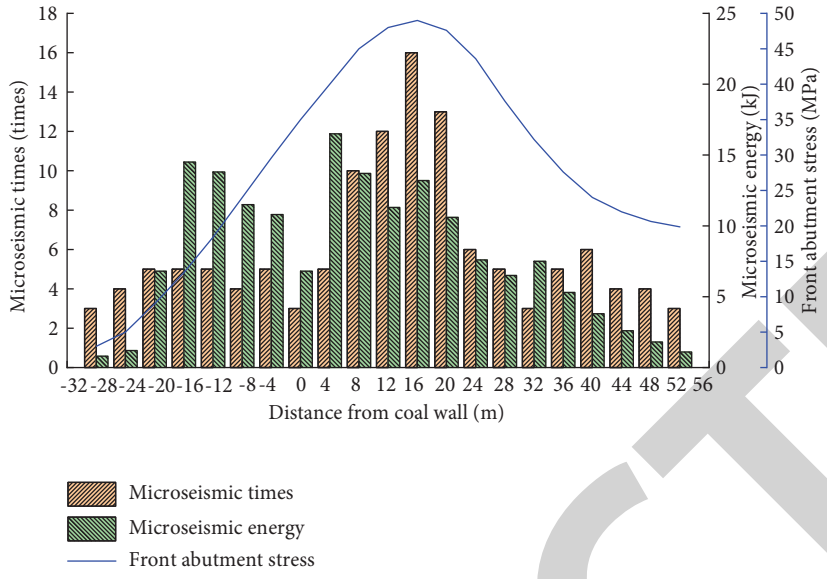

(e)

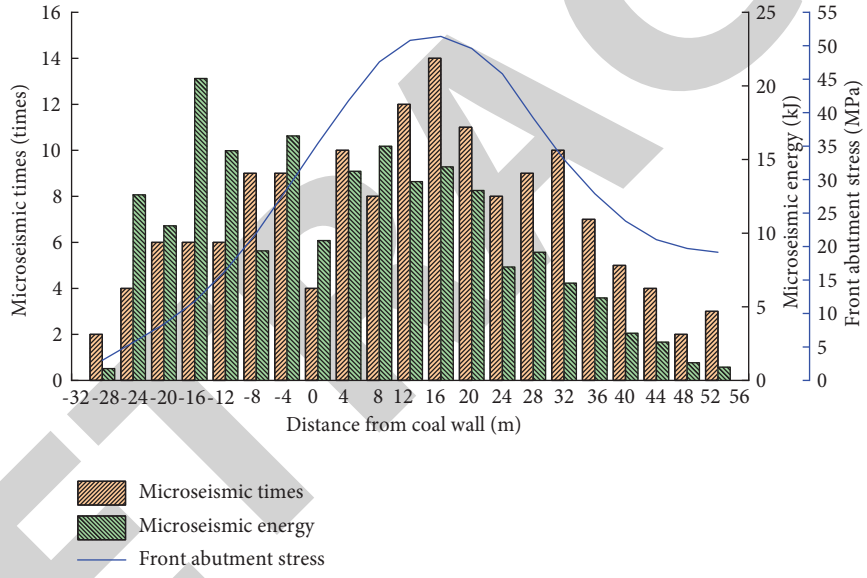

(f)

Figure 5: Continued.

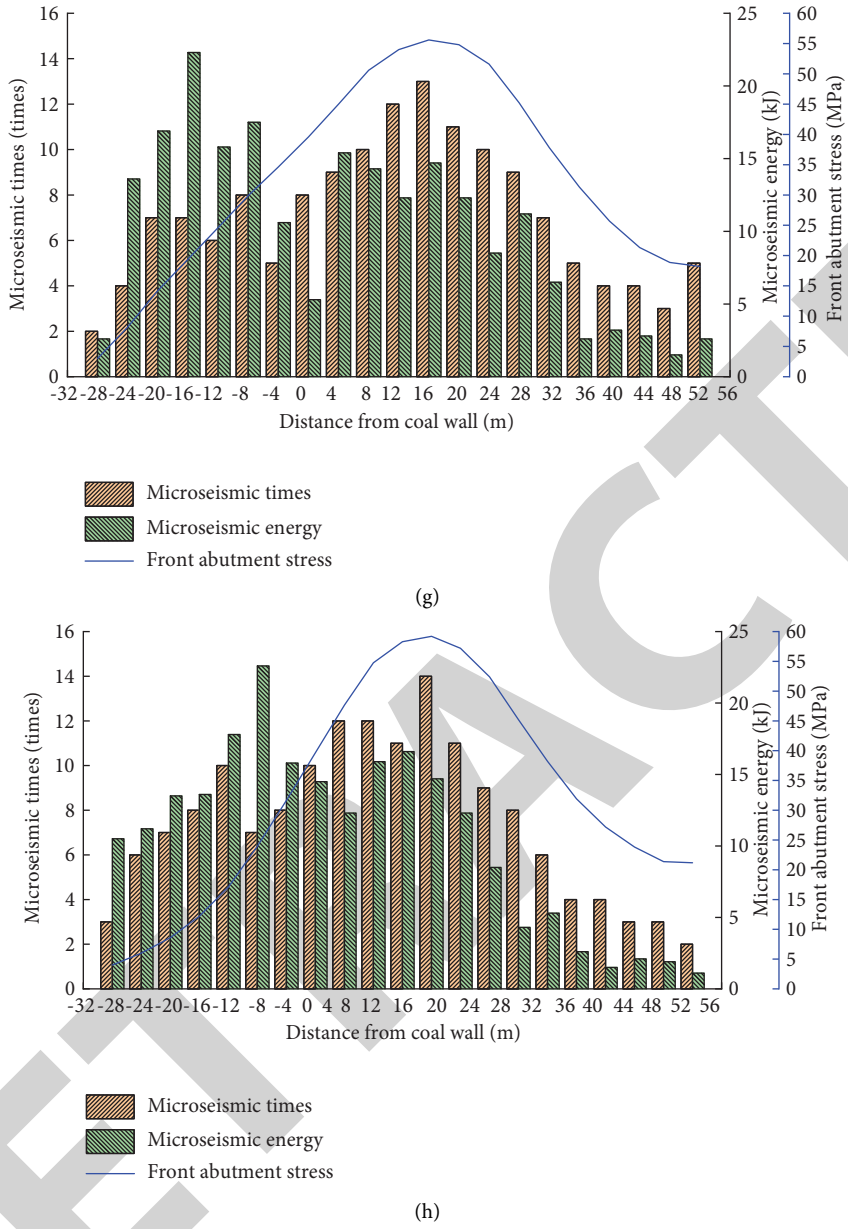

Figure 5: Relationship between microseismic frequency, energy, and support pressure. (a) Caving 50 m. (b) Caving 100 m. (c) Caving 150 m. (d) Caving 200 m. (e) Caving 250 m. (f) Caving 300 m. (g) Caving 350 m. (h) Caving 400 m.

events [39]. The occurrence of microseismic events was the reaction of failure of roof and floor surrounding rocks. The level of microseismic events was a mapping of failure degree of surrounding rocks [40]. The fracture degree of surrounding rock was also basis for the division of three zones on the working face. So, the height of overlying rock three zones was divided according to the microseismic level and density. Taking the 1305 working face as an example, all microseismic events were projected to the vertical section when the working face was mined to 176 m. Then, the height of caving zone and fracture zone were inferred according to the microseismic distribution in Figure 7. The results show that the height of caving zone is 37.8 m, and it is 4.97 times as large as the coal seam (the thickness of coal seam is 7.6 m). The height of fracture zone is 95 m. It is about 12.50 times as large as the coal seam thickness. The microseismic events were mostly distributed in the caving zone and fracture zone, and it is mainly in the fracture zone. The microseismic hypocenter was mainly in the advance of the working face 100 m and it is behind the coal rib 150 m.

To further determine the accuracy of overlying rock, two zones height was obtained by a microseismic monitoring method. The microseismic monitoring results were compared with the numerical calculation results in Figure 8. The results show that the overlying rock fracture height is 87 m when the working face was mining to 200 m in the numerical simulation (Figure 8(d)). It is 8.4% smaller than the

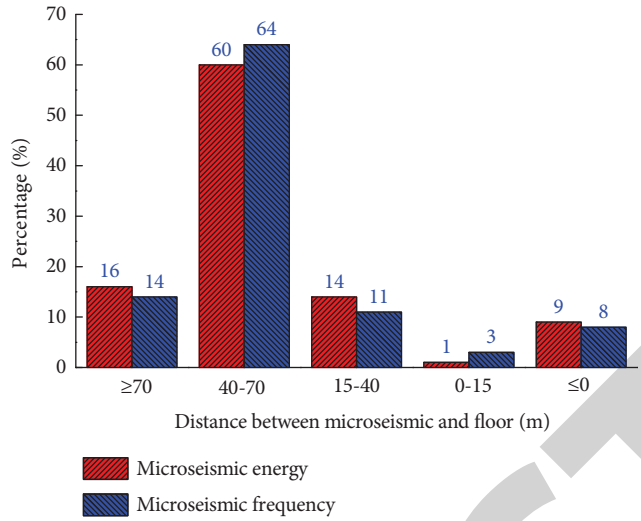

Figure 6: Distribution of microseismic energy and frequency in different layers.

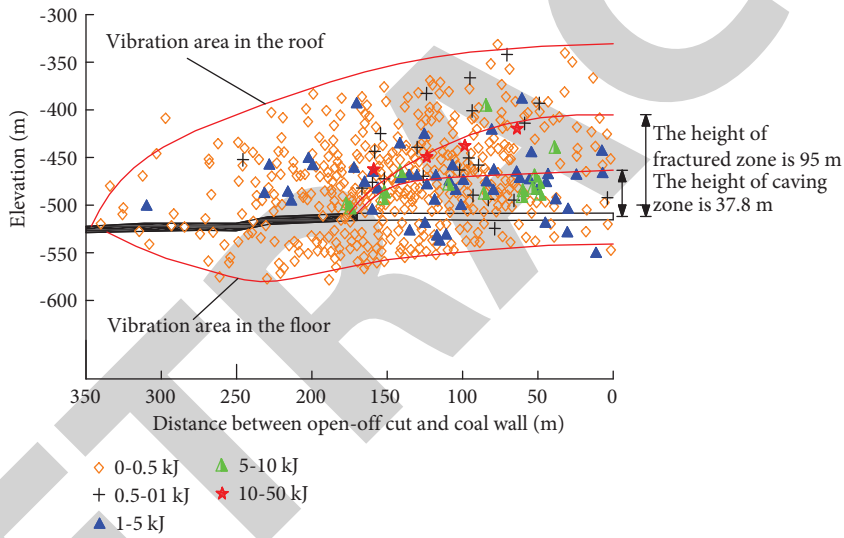

Figure 7: Height of the caving zone and fracture zone revealed by microseismic events.

microseismic monitoring result. Therefore, it is considered that the accuracy of mining two zones of overlying rock based on the microseismic monitoring was better and it can be used in the field.

5. Analysis of the Coal Mine Earthquake Gestation Process Based on the Burgers Model

The occurrence of coal mine earthquake was transient, which is the process of instantaneous instability of rock medium in hypocenter area [41]. The rock in the hypocenter area was broken, the rock mass was staggered, the violent appearance of mine pressure, and it was a threat to the safety of working face equipment and personnel in the working face when the coal mine earthquake occurs [42]. However, it is different from the transient process of coal mine earthquake and the gestation of coal mine earthquake needs a long time. Therefore, for the gestation of coal mine earthquake process under slow loading, the changes of stress, strain, energy, and strain rate of rock will be shown as the accumulation process of flow variation to a certain extent [43]. Therefore, the rheological characteristics of rock medium can be used to describing the gestation process of coal mine earthquakes. The change law with the time of physical quantities such as stress, strain, strain rate, and energy and the precursory information of coal mine earthquakes were analyzed in the gestation process of coal mine earthquakes. The Burgers model was selected to simulating the rheological properties of hypocenter region and its surrounding rock medium during the gestation of coal mine earthquake. The Burgers model is a combination of the Kelvin model and the Maxwell model as shown in Figure 9 [44]. The E_1 and η_1, respectively, represent the elastic modulus of elastic element and the viscosity coefficient of viscous element in the Maxwell model in Figure 9.

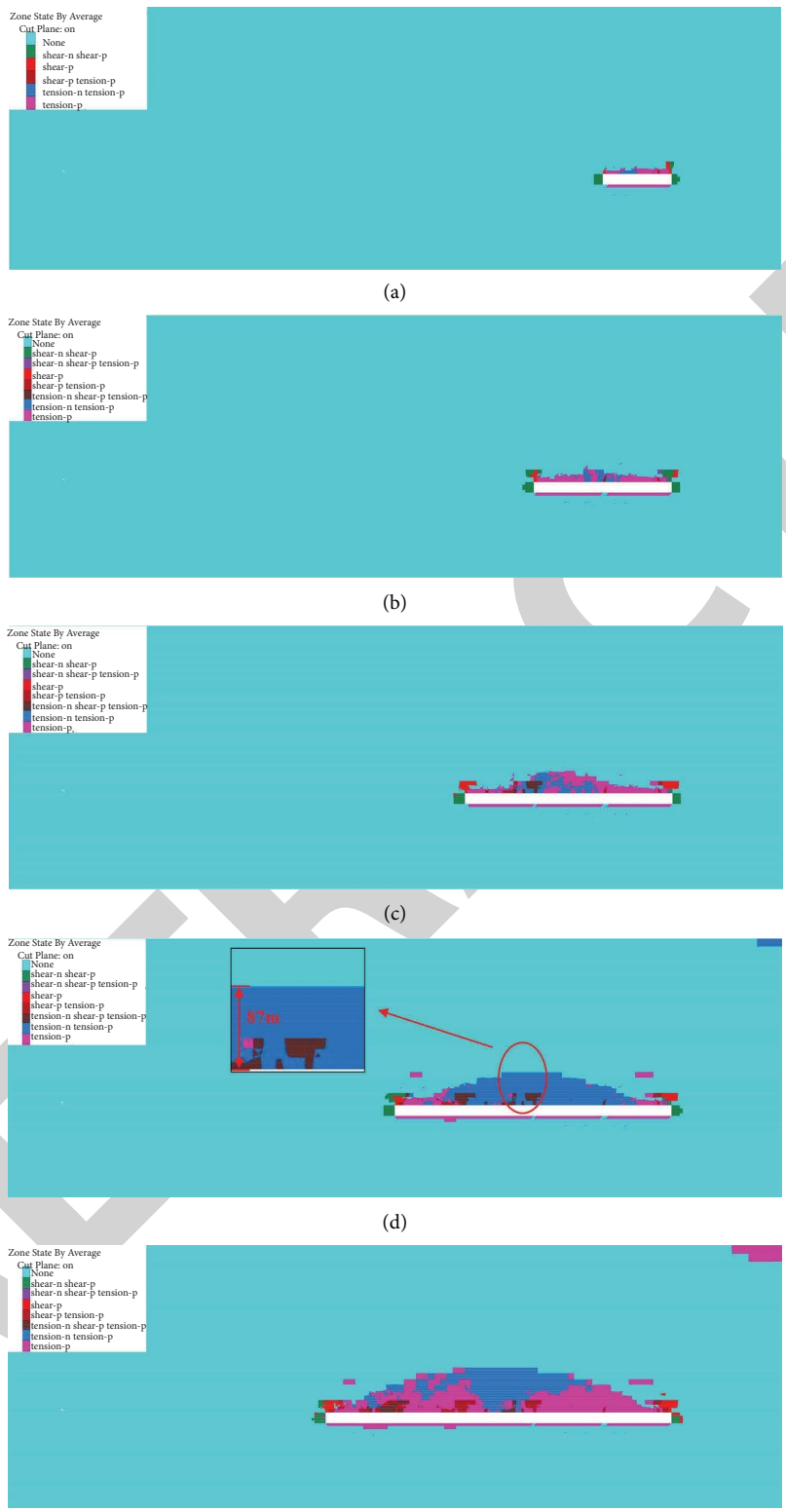

Figure 8: Continued.

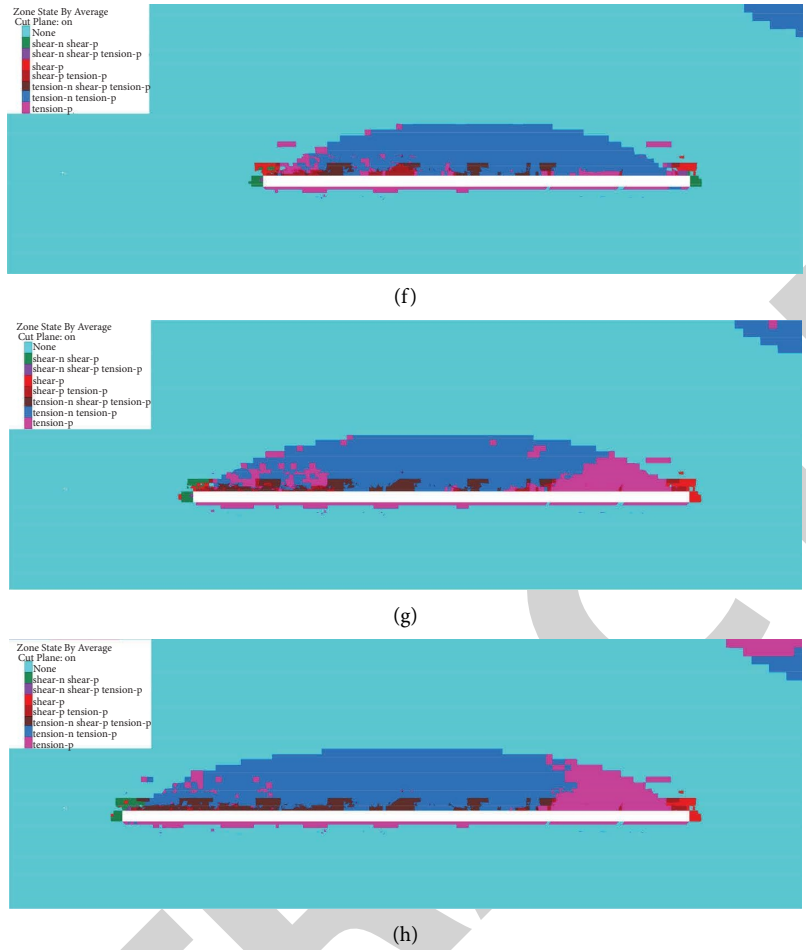

Figure 8: Fracture height of overlying rock revealed by numerical simulation. (a) Caving 50 m. (b) Caving 100 m. (c) Caving 150 m. (d) Caving 200 m. (e) Caving 250 m. (f) Caving 300 m. (g) Caving 350 m. (h) Caving 400 m.

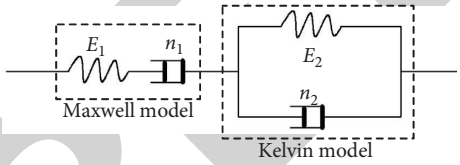

Figure 9: Physical composition of the Burgers model.

The E_2 and η_2, respectively, represent the elastic modulus of elastic element and the viscosity coefficient of viscous element in the Kelvin model.

The gestation process of coal mine earthquake was a growth process of stress, strain, and energy in the hypocenter area. The coal mine earthquake occurred when the stress or energy in the hypocenter area reaches critical stress or energy of coal mine earthquake [45–48]. The strain growth in the hypocenter area during gestation of coal mine earthquakes includes the elastic strain and inelastic strain [49]. The time history curves of stress, strain, energy, and strain rate during gestation of coal mine earthquake in Figure 10. The ε, σ, W, $\dot{\varepsilon}$, and t represent total strain, stress, energy, strain rate, and time, respectively, in the Burgers model. The ε_{11}, ε_{12}, σ_{11}, σ_{12}, W_{11}, W_{12}, $\dot{\varepsilon}_{11}$, and $\dot{\varepsilon}_{12}$, respectively, represent elastic element strain, viscous element strain, elastic element stress, viscous element stress, elastic element energy, viscous element energy, elastic element strain rate, and viscous element strain rate in the Maxwell model. The ε_{21}, ε_{22}, σ_{21}, σ_{22}, W_{21}, W_{22}, $\dot{\varepsilon}_{21}$, and $\dot{\varepsilon}_{22}$, respectively, represent elastic element strain, viscous element strain, elastic element stress, viscous element stress, elastic element energy, viscous element energy, elastic element strain rate, and viscous element strain rate in the Kelvin model. It can be seen that the early stage of coal mine earthquake was mainly stage of elastic strain accumulation; the system energy mainly manifested the increase of elastic energy. This is because the inelastic deformation was not obvious at this stage. It is ignored when the work of the viscous element is very small. The later stage of coal mine earthquake gestation was the rapid growth stage of inelastic deformation. The inelastic deformation done work increases rapidly with increase of inelastic strain. In the high stress (energy) stage the occurrence of near the coal mine earthquake. The dissipation of inelastic energy has an accelerating upward trend with rapid growth of various forms of inelastic

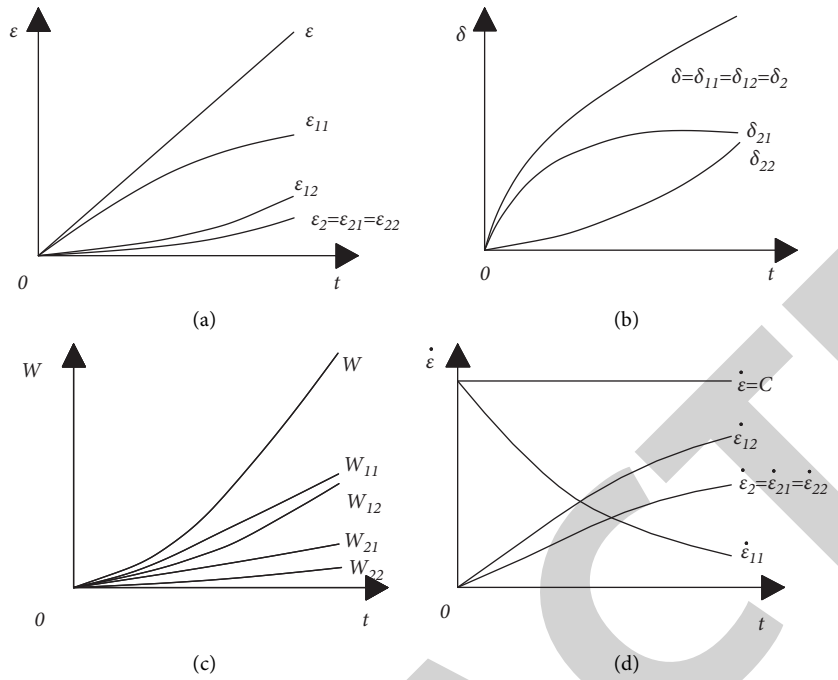

Figure 10: Curves of stress, strain, strain rate, and energy during the coal mine earthquake gestation process. (a) Time history curve of strain. (b) Time history curve of stress. (c) Time history curve of energy. (d) Time history curve of strain rate.

deformation including development of t microcracks, plastic deformation, and fault creep. The ultimate condition of occurrence of coal mine earthquake was reached finally. The huge cumulative energy was released in an instant and the large energy coal mine earthquake occurs.

6. Conclusion

The engineering effect of working face mining (mainly includes distribution of mining stress and fracture characteristics of overlying rock) were comprehensively studied by theoretical analysis, numerical simulation, microseismic monitoring, and other means in this paper. The disaster-pregnant mechanism of disastrous coal mine earthquakes was analyzed. The research results provided reference for prevention and control of dynamic disasters in the coal mining. The main conclusions of this paper are as follows.

(1) The hypocenter point always accumulates in front of the working face and behind the goaf, and it is more in front of working face than behind the goaf. The fracture zone and stress increase area are mainly concentrated. The hypocenter point first accumulates at the main roof with advance of working face. Then, it gradually develops upward and then decreases to near the main roof after mining. The hypocenter points are mainly distributed in the vertical stress increase areas and vertical stress decrease areas.

(2) The trend of microseismic frequency and support pressure distribution is basically consistent. The microseismic energy peak value area with respect to support pressure peak value area often presents a certain lag. The empirical formula of relationship was inferred as $Y_E = M_E + \Delta d$.

(3) The height of overlying rock caving zone revealed is 37.8 m by microseismic monitoring. It is 4.97 times as large as the coal seam. The height of fracture zone is 95 m. It is about 12.50 times as large as the coal seam thickness. It is roughly consistent with numerical results. The microseismic hypocenter was mainly in the advance working face 100 m and behind the coal rib 150 m.

(4) The research study on the mechanism of coal mine earthquake gestation shows as follows. The gestation of coal mine earthquake experienced the stage of elastic strain accumulation and stage of inelastic strain accumulation. The high stress environment promotes rapid growth of inelastic strain and acceleration of energy consumption. The coal mine earthquake reaches the limit condition of coal mine earthquake after mining disturbance. The energy was released instantaneously and the large coal mine earthquake occurs.

Data Availability

All data generated or analyzed during this study are included within this article.

Conflicts of Interest

The authors declare that there are no conflicts of interest regarding the publication of this paper.

Acknowledgments

The study of this paper was supported by the National Natural Science Foundation of China (No. 52064043), the Natural Science Foundation of Inner Mongolia Autonomous Region (No. 2019LH05005), and the Innovation Foundation of Inner Mongolia University of Science and Technology (No. 2019QDL-B32).

References

[1] J. Z. Li, P. H. Guo, H. Cui et al., "Dynamic response mechanism of impact instability induced by dynamic load disturbance to surrounding rock in high static loading roadway," *Minerals*, vol. 11, no. 9, 2021.

[2] Y. Liu, F. Y. Jiang, and Y. Feng, "Study of occurrence mechanism and risk analysis of induced rockburst in roadway," *Rock and Soil Mechanics*, vol. 36, no. S2, pp. 201–207+220, 2015.

[3] T. B. Zhao, W. Y. Guo, Y. L. Tan, Y. C. Yin, L. S. Cai, and J. F. Pan, "Case studies of rock bursts under complicated geological conditions during multi-seam mining at a depth of 800 m," *Rock Mechanics and Rock Engineering*, vol. 51, no. 5, pp. 1539–1564, 2018.

[4] P. F. Lyu, F. Ma, and X. Y. Bao, "Experimental study on pore microstructure and methane occurrence characteristics of shale of marine-continent transition phase," *Fresenius Environmental Bulletin*, vol. 30, no. 1, pp. 330–337, 2021.

[5] L. Pengfei, B. Xinyang, L. Gang, and C. Xuehua, "Research on fault activation law in deep mining face and mechanism of rockburst induced by fault activation," *Advances in Civil Engineering*, vol. 2020, Article ID 8854467, 13 pages, 2020.

[6] P. F. Lyu, *Research on disaster-causing characteristics of rock burst induced by disturbance loading and its integration prevention technology*, Ph.D. Thesis, Liaoning Technical University Fuxin, China, 2018.

[7] B. Wang, *Mechanism and control of typical dynamic disasters in deep mining areas of Shanxi and Inner Mongolia*, Ph.D. Thesis, University of Science and Technology Beijing, Beijing, China, 2021.

[8] Y. Z. Li, *Study on mechanism and prevention method of coal bump controlled by large geological body*, Ph.D Thesis, China Coal Research Institute, Beijing, China, 2021.

[9] A. Kidybiński, "Bursting liability indices of coal," *International Journal of Rock Mechanics and Mining Sciences & Geomechanics Abstracts*, vol. 18, no. 4, pp. 295–304, 1981.

[10] S. P. Singh, "Burst energy release index," *Rock Mechanics and Rock Engineering*, vol. 21, no. 2, pp. 149–155, 1988.

[11] P. F. Lyu, X. H. Chen, G. B. Chen, and L. Qiu, "Experimental study on dynamic mechanical responses of coal specimens under the combined dynamic-static loading," *Arabian Journal of Geosciences*, vol. 13, no. 18, p. 935, 2020.

[12] Z. J. Zhu, Y. L. Wu, and Z. Liang, "Mining-induced stress and ground pressure behavior characteristics in mining a thick coal seam with hard roofs," *Frontiers of Earth Science*, vol. 10, Article ID 843191, 2022.

[13] Z. J. Zhu, Y. L. Wu, and J. Han, "A prediction method of coal burst based on analytic hierarchy process and fuzzy comprehensive evaluation," *Frontiers of Earth Science*, vol. 9, Article ID 834958, 2022.

[14] L. Pengfei and C. Xuekai, "Mechanism of vibration energy action on dynamic instability of shock-type rockburst carrier system," *Shock and Vibration*, vol. 2020, Article ID 6663269, 10 pages, 2020.

[15] L. Pengfei, L. Jiabin, W. Eryu, and C. Xuehua, "The mechanical criterion of activation and instability of normal fault induced by the movement of key stratum and its disaster-causing mechanism of rockburst in the hanging wall mining," *Advances in Civil Engineering*, vol. 2021, Article ID 6618957, 11 pages, 2021.

[16] G. Y. Wang, L. M. Dou, Z. L. Li, S. Y. Gong, J. He, and W. Cai, "Space breeding mechanism of rock burst and its microseismic characteristics," *Journal of Mining & Safety Engineering*, vol. 31, no. 1, pp. 41–48, 2014.

[17] Z. L. Li, L. M. Dou, W. Cai et al., "Investigation and analysis of the rock burst mechanism induced within fault-pillars," *International Journal of Rock Mechanics and Mining Sciences*, vol. 70, pp. 192–200, 2014.

[18] W. Cai, L. M. Dou, Z. L. Li, J. He, H. He, and Y. Ding, "Mechanical initiation and propagation mechanism of a thrust fault: a case study of the Yima section of the Xiashi-Yima thrust (North side of the eastern Qinling orogen, China)," *Rock Mechanics and Rock Engineering*, vol. 48, no. 5, pp. 1927–1945, 2015.

[19] J. F. Pan, S. H. Liu, S. W. Wang, and Y. X. Xia, "A new theoretical view of rockburst and its engineering application," *Advances in Civil Engineering*, vol. 2018, Article ID 4683457, 12 pages, 2018.

[20] J. F. Pan, S. H. Liu, J. M. Gao, X. K. Sun, Y. X. Xia, and Q. Wang, "Prevention theory and technology of rock burst with distinguish dynamic and static load sources in deep mine roadway," *Journal of China Coal Society*, vol. 45, no. 5, pp. 1607–1613, 2020.

[21] L. H. Kong, "Relationship between microseismic events and abutment pressure distribution in coal mining," *Journal of Mining & Safety Engineering*, vol. 31, no. 4, pp. 525–531, 2014.

[22] S. H. Wang, D. B. Mao, J. F. Pan, J. G. Chen, F. B. Chen, and H. Lan, "Measurement on the whole process of abutment pressure evolution and microseismic activities at the lateral strata of goaf," *Journal of China Coal Society*, vol. 40, no. 12, pp. 2772–2779, 2015.

[23] Q. W. Shi, B. Mishra, S. W. Wang, and G. Xu, "In Situ Assessment of the effectiveness of an undisturbed single driving entry's relief borehole in coal burst-prone seam," *Mining Metallurgy & Exploration*, vol. 38, no. 6, pp. 2443–2452, 2021.

[24] W. J. Ju, L. W. Sun, S. H. Liu, S. W. Wang, and T. T. Du, "Idea and implementation of stress relief-support reinforcement cooperative control in rockburst roadway," *Coal Science and Technology*, vol. 49, no. 4, pp. 90–94, 2021.

[25] J. F. Pan, Q. X. Qi, S. H. Liu, S. W. Wang, W. T. Ma, and X. C. Kang, "Characteristics, types and prevention and control technology of rock burst in deep coal mining in China," *Journal of China Coal Society*, vol. 45, no. 1, pp. 111–121, 2020.

[26] W. Cai, L. M. Dou, Z. L. Li, S. Y. Gong, R. J. Han, and J. Liu, "Verification of passive seismic velocity tomography in rock burst hazard assessment," *Chinese Journal of Geophysics-Chinese Edition*, vol. 59, no. 1, pp. 252–262, 2016.

[27] W. Cai, L. M. Dou, G. Y. Si, and Y. W. Hu, "Fault-induced coal burst mechanism under mining-induced static and dynamic stresses," *Engineering*, vol. 7, no. 5, pp. 687–700, 2021.

[28] W. Cai, X. X. Bai, G. Y. Si, W. Z. Cao, S. Y. Gong, and L. M. Dou, "A monitoring investigation into rock burst mechanism based on the coupled theory of static and dynamic stresses," *Rock Mechanics and Rock Engineering*, vol. 53, no. 12, pp. 5451–5471, 2020.

[29] B. B. Gao, H. G. Li, H. M. Li, R. F. Yuan, and Y. P. Liu, "Current situation of the study on acoustic emission and microseismic monitoring of coupling dynamic catastrophe

for gas-filled coal-rock," *Progress in Geophysics*, vol. 29, no. 2, pp. 689–697, 2014.

[30] X. Yin, Q. S. Liu, X. Huang, and Y. C. Pan, "Real-time prediction of rockburst intensity using an integrated CNN-Adam-BO algorithm based on microseismic data and its engineering application," *Tunnelling and Underground Space Technology*, vol. 117, Article ID 104133, 2021.

[31] Y. C. Wang, C. A. Tang, L. X. Tang et al., "Microseismicity characteristics before and after a rockburst and mechanisms of intermittent rockbursts in a water diversion tunnel," *Rock Mechanics and Rock Engineering*, vol. 55, no. 1, pp. 341–361, 2021.

[32] Y. T. Sun, G. C. Li, J. F. Zhang, and J. D. Huang, "Rockburst intensity evaluation by a novel systematic and evolved approach: machine learning booster and application," *Bulletin of Engineering Geology and the Environment*, vol. 80, no. 11, pp. 8385–8395, 2021.

[33] D. Chlebowski and Z. Burtan, "Mining-induced seismicity during development works in coalbeds in the context of forecasts of geomechanical conditions," *Energies*, vol. 14, no. 20, p. 6675, 2021.

[34] J. C. Wang, G. Q. Chen, Y. X. Xiao, S. J. Li, Y. Chen, and Z. B. Qiao, "Effect of structural planes on rockburst distribution: case study of a deep tunnel in Southwest China," *Engineering Geology*, vol. 292, Article ID 106250, 2021.

[35] X. L. Li, S. J. Chen, E. Y. Wang, and Z. H. Li, "Rockburst mechanism in coal rock with structural surface and the microseismic (MS) and electromagnetic radiation (EMR) response," *Engineering Failure Analysis*, vol. 124, Article ID 105396, 2021.

[36] M. M. He, Z. Q. Zhang, J. W. Zhu, N. Li, G. F. Li, and Y. S. Chen, "Correlation between the rockburst proneness and friction characteristics of rock materials and a new method for rockburst proneness prediction: field demonstration," *Journal of Petroleum Science and Engineering*, vol. 205, Article ID 108997, 2021.

[37] H. S. Aghamiry, A. Gholami, S. Operto, and A. Malcolm, "ADMM-based full-waveform inversion for microseismic imaging," *Geophysical Journal International*, vol. 228, no. 1, pp. 259–274, 2021.

[38] A. M. Dichiarante, N. Langet, R. A. Bauer et al., "Identifying geological structures through microseismic cluster and burst analyses complementing active seismic interpretation," *Tectonophysics*, vol. 820, Article ID 229107, 2021.

[39] H. Y. Gao, M. R. Zhang, N. Hou, and H. L. Dong, "Dynamic-transmission-based recursive filtering algorithm for microseismic event detection under sensor saturations," *Measurement*, vol. 186, Article ID 110197, 2021.

[40] Z. Zarifi, F. Hansteen, and F. Schopper, "Seismic moment tensor inversion of an induced microseismic event offshore Norway: an insight into the possible cause of wellbore liner failure during a drilling operation," *Seismological Research Letters*, vol. 92, no. 6, pp. 3460–3470, 2021.

[41] X. Liu, Q. S. Liu, Y. C. Pan, and X. Huang, "A novel tree-based algorithm for real-time prediction of rockburst risk using field microseismic monitoring," *Environmental Earth Sciences*, vol. 80, no. 16, 2021.

[42] F. Feng, X. B. Li, L. Luo et al., "Rockburst response in hard rock owing to excavation unloading of twin tunnels at great depth," *Bulletin of Engineering Geology and the Environment*, vol. 80, no. 10, pp. 7613–7631, 2021.

[43] M. Javaid, M. Tahir, M. Imran, D. Baleanu, A. Akgul, and M. A. Imran, "Unsteady flow of fractional Burgers' fluid in a rotating annulus region with power law kernel," *Alexandria Engineering Journal*, vol. 61, no. 1, pp. 17–27, 2022.

[44] K. J. Wang, "Generalized variational principle and periodic wave solution to the modified equal width-Burgers equation in nonlinear dispersion media," *Physics Letters A*, vol. 419, Article ID 127723, 2021.

[45] X. Yin, Q. S. Liu, Y. C. Pan, and X. Huang, "A novel tree-based algorithm for real-time prediction of rockburst risk using field microseismic monitoring," *Environmental Earth Sciences*, vol. 80, no. 16, p. 504, 2021.

[46] L. B. Song, Q. Jiang, Z. Zhong et al., "Technical path of model reconstruction and shear wear analysis for natural joint based on 3D scanning technology," *Measurement*, vol. 188, Article ID 110584, 2022.

[47] L. B. Song, G. Wang, X. K. Wang et al., "The influence of joint inclination and opening width on fracture characteristics of granite under triaxial compression," *International Journal of Geomechanics*, vol. 22, no. 5, Article ID 04022031, 2022.

[48] Y. Luo, G. Wang, X. P. Li et al., "Analysis of energy dissipation and crack evolution law of sandstone under impact load," *International Journal of Rock Mechanics and Mining Sciences*, vol. 132, Article ID 104359, 2020.

[49] A. Schulze-Halberg, "A new type of Darboux transformations for the one-dimensional Burgers equation with forcing," *Physica Scripta*, vol. 96, no. 12, Article ID 125247, 2021.